

Three-loop induced neutrino mass model in a non-invertible symmetry

Hiroshi Okada^{1,*} and Yoshihiro Shigekami^{1,†}

¹*Department of Physics, Henan Normal University, Xinxiang 453007, China*

(Dated: July 23, 2025)

We propose a new type of radiatively induced neutrino masses at three-loop level based on the Ma model, introducing a non-invertible symmetry in the class under a \mathbb{Z}_2 gauging of \mathbb{Z}_6 symmetry and adding three isospin doublet vector-like fermions L' and singlet boson S_0 . Under this symmetry, the Yukawa interactions directly related to the neutrino masses are not allowed at tree-level. However it is allowed at one-loop level due to L' and S_0 as well as η , which is no longer invariant under this symmetry. Therefore, the symmetry is dynamically broken. Intriguingly, η plays important roles in contributing to both the radiative matrices y^η and m_ν . After constructing our model, we show some numerical analyses to satisfy the lepton flavor violations, muon anomalous magnetic dipole moment, and a boson dark matter candidate S_0 or η_R for the cases of normal hierarchy and inverted hierarchy. Then, we demonstrate allowed space for our input parameters.

PACS numbers:

*Electronic address: hiroshi3okada@htu.edu.cn

†Electronic address: shigekami@htu.edu.cn

I. INTRODUCTION

Non-invertible symmetries possess an intriguing nature that the symmetry can dynamically be broken at loop levels even though it is symmetric under the tree level. Also, they have a kind of group theory such as \mathbb{Z}_N symmetry. Thus, several literatures [1–16] are recently appeared, applying these symmetries to phenomenology such as radiatively induced mass matrices, zero texture's realizations of mass matrices, mass eigenvalues and mixing angles, CP phases in quark and lepton sectors. Although these symmetries are not groups, they are supported by some formal theories; the worldsheet theory of perturbative string theory [17], heterotic string theory on toroidal orbifolds [18–24], Calabi-Yau threefolds [25], and type II intersecting/magnetized D-brane models [6, 26].

In this work, we apply a non-invertible symmetry in a class under \mathbb{Z}_2 gauging of \mathbb{Z}_6 symmetry to a radiative seesaw model, which is sometimes called Ma model [27]. The Yukawa coupling to generate the neutrino mass matrix is forbidden at the tree level due to this invertible symmetry, but it is induced at one-loop level.

It would be helpful to start a brief review on the Ma model before discussing our model. The model provides the neutrino mass matrix at one-loop level, introducing the right-handed neutral fermions N_R and an isospin doublet inert boson $\eta (\equiv [\eta^+, (\eta_R + i\eta_I)/\sqrt{2}]^T)$. In addition, \mathbb{Z}_2 symmetry is imposed in order to forbid the tree-level neutrino mass matrix. The field contents and their charge assignments are listed in Table I. Clearly, only new fields are assigned by \mathbb{Z}_2 odd. Under the symmetry, the valid terms to induce the neutrino mass matrix as well as the charged-lepton masses are found as

$$y_i^\ell \bar{L}_{L_i} H \ell_{R_i} + y_{ia}^\eta \bar{L}_{L_i} \tilde{\eta} N_{R_a} + M_{N_a} \bar{N}_{R_a}^C N_{R_a} + \lambda_{H\eta}'' (H^\dagger \eta)^2 + \text{h.c.}, \quad (1)$$

where y^ℓ and M_N can be diagonal without loss of generality, and $\tilde{\eta} \equiv i\sigma_2 \eta^*$ being σ_2 second Pauli matrix. The resultant neutrino mass matrix is then given by

$$(m_\nu)_{ij} = \sum_{a=1}^3 \frac{y_{ia}^\eta M_{N_a} y_{ja}^\eta}{(4\pi)^2} \left[\frac{m_R^2}{m_R^2 - M_{N_a}^2} \ln \left(\frac{m_R^2}{M_{N_a}^2} \right) - \frac{m_I^2}{m_I^2 - M_{N_a}^2} \ln \left(\frac{m_I^2}{M_{N_a}^2} \right) \right] \equiv y_{ia}^\eta D_{N_a} y_{ja}^\eta, \quad (2)$$

where m_R and m_I are respectively mass eigenvalues of η_R and η_I . Note that the mass difference between η_R and η_I leads us to the non-vanishing neutrino masses and its difference arises from $\lambda_{H\eta}''$. The neutrino mass matrix is diagonalized by a unitary matrix U_ν as $D_\nu \equiv U_\nu^T m_\nu U_\nu$. Moreover, since the mass matrix of charged-lepton is diagonal, U_ν is identified by the lepton mixing matrix $U = U_{\text{PMNS}}$ which could be observed. Following the Casas-Ibarra parametrization [28], we can

	L_L	ℓ_R	N_R	H	η
$SU(2)_L$	2	1	1	2	2
$U(1)_Y$	$-\frac{1}{2}$	-1	0	$\frac{1}{2}$	$\frac{1}{2}$
\mathbb{Z}_2	$+$	$+$	$-$	$+$	$-$

TABLE I: The Ma model; charge assignments of the fermions and bosons under $SU(2)_L \otimes U(1)_Y \otimes \mathbb{Z}_2$, where we assume all fermions have three families.

rewrite y^η in terms of observed and some parameters as

$$y^\eta = U^* \sqrt{D_\nu} O_N \left(\sqrt{D_N} \right)^{-1}, \quad (3)$$

where the y^η has to satisfy the perturbative limit $\text{Max}[|y^\eta|] \lesssim 4\pi$, and O_N is an orthogonal mixing matrix $O_N O_N^T = O_N^T O_N = \mathbb{I}$ with three complex free parameters. The neutrino mass eigenvalues are written in terms of two observables ($\Delta m_{\text{atm}}^2, \Delta m_{\text{sol}}^2$) and the lightest neutrino mass eigenvalue as follows:

$$\text{NH} : D_{\nu_2} = \sqrt{\Delta m_{\text{sol}}^2 + D_{\nu_1}^2}, \quad D_{\nu_3} = \sqrt{\Delta m_{\text{atm}}^2 + D_{\nu_1}^2}, \quad (4)$$

$$\text{IH} : D_{\nu_1} = \sqrt{\Delta m_{\text{atm}}^2 - \Delta m_{\text{sol}}^2 + D_{\nu_3}^2}, \quad D_{\nu_2} = \sqrt{\Delta m_{\text{atm}}^2 + D_{\nu_3}^2}, \quad (5)$$

where NH (IH) is an abbreviated notation of normal hierarchy (inverted hierarchy).

There are several experimental constraints on the model. First, the sum of neutrino masses, which is denoted by $\sum D_\nu = D_{\nu_1} + D_{\nu_2} + D_{\nu_3}$, is constrained by the minimal standard cosmological model with CMB data as $\sum D_\nu \leq 120$ meV [29]. Second, the effective mass for neutrinoless double beta decay m_{ee} is defined as

$$m_{ee} = \left| D_{\nu_1} c_{12}^2 c_{13}^2 + D_{\nu_2} s_{12}^2 c_{13}^2 e^{i\alpha_{21}} + D_{\nu_3} s_{13}^2 e^{i(\alpha_{31} - 2\delta_{CP})} \right|, \quad (6)$$

where $s_{12,23,13}(c_{12,23,13})$, which are short-hand notations $\sin \theta_{12,23,13}(\cos \theta_{12,23,13})$, are neutrino mixing of U , δ_{CP} is Dirac phase, $\alpha_{21,31}$ are Majorana phases. The upper bound on m_{ee} is provided by the current KamLAND-Zen data measured in the future [30]; $m_{ee} < (36 - 156)$ meV at 90 % confidence level (CL). Moreover, $m_{\nu e}$ is given by

$$m_{\nu e} = \sqrt{D_{\nu_1}^2 c_{13}^2 c_{12}^2 + D_{\nu_2}^2 c_{13}^2 s_{12}^2 + D_{\nu_3}^2 s_{13}^2}. \quad (7)$$

whose upper bound is given by KATRIN [31]; $m_{\nu e} \leq 450$ meV at 90% CL, which is weaker than $\sum D_\nu$ and m_{ee} . In addition to constraints on the neutrino sector, we should care about those on the charged lepton sector in this kind of models, induced by y^η . The crucial constraints are coming

from lepton flavor violation (LFV) processes and the muon anomalous magnetic moment ($g - 2$), and their formulae are found as

$$\text{BR}(\ell_i \rightarrow \ell_j \gamma) \approx \frac{48\pi^3 \alpha_{em} C_{ij}}{G_F^2 m_{\ell_i}^2} (|(a_R)_{ij}|^2 + |(a_L)_{ij}|^2), \quad (8)$$

$$\Delta a_\mu \approx -m_\mu [(a_R)_{22} + (a_L)_{22}], \quad (9)$$

where $\ell_1 \equiv e$, $\ell_2 \equiv \mu$, and $\ell_3 \equiv \tau$, α_{em} is fine-structure constant, G_F is Fermi constant, $C_{21} = 1$, $C_{31} = 0.1784$, and $C_{21} = 0.173648$. a_R and a_L are given by

$$(a_R)_{ij} \approx \sum_{a=1}^3 \frac{y_{ja}^\eta (y^\eta)_{ai}^\dagger m_{\ell_i}}{12(4\pi)^2} \left[\frac{M_{N_a}^6 - 6M_{N_a}^4 m_\eta^2 + 3M_{N_a}^2 m_\eta^4 + 2m_\eta^6 + 6M_{N_a}^2 m_\eta^4 \ln\left(\frac{M_{N_a}^2}{m_\eta^2}\right)}{(M_{N_a}^2 - m_\eta^2)^4} \right], \quad (10)$$

$$(a_L)_{ij} \approx \sum_{a=1}^3 \frac{y_{ja}^\eta (y^\eta)_{ai}^\dagger m_{\ell_j}}{12(4\pi)^2} \left[\frac{M_{N_a}^6 - 6M_{N_a}^4 m_\eta^2 + 3M_{N_a}^2 m_\eta^4 + 2m_\eta^6 + 6M_{N_a}^2 m_\eta^4 \ln\left(\frac{M_{N_a}^2}{m_\eta^2}\right)}{(M_{N_a}^2 - m_\eta^2)^4} \right], \quad (11)$$

where m_η is the mass eigenvalue of η^\pm . The experimental upper bounds are respectively given by

$$\text{BR}(\mu \rightarrow e \gamma) \lesssim 3.1 \times 10^{-13}, \quad \text{BR}(\tau \rightarrow e \gamma) \lesssim 3.3 \times 10^{-8}, \quad \text{BR}(\tau \rightarrow \mu \gamma) \lesssim 4.4 \times 10^{-8}. \quad (12)$$

Recent measurement of muon $g - 2$ includes the prediction of the Standard Model (SM) [32, 33], and it is given within 1σ as

$$\Delta a_\mu \simeq (39 \pm 64) \times 10^{-11}. \quad (13)$$

Now that experimental value allows both the sign of muon $g - 2$, and the theory suggests negative. Therefore, it would be verifiable in the near future.

It is notable that there are two dark matter (DM) candidates in the model: N_{R_1} or η_R . If the DM is fermion N_{R_1} , the main annihilation to explain the relic density of DM is arisen from Yukawa coupling y^η [34], and only when $y^\eta = \mathcal{O}(1)$, it reaches the observed relic density [35]. Note that since N_{R_1} does not couple to quark sector at the tree-level, one can easily evade constraints of direct detection searches. In the case where the DM is η_R , the main cross section would come from kinetic terms [36]¹, which results in mostly fixed DM mass as

$$m_R \approx 534 \pm 8.5 \text{ GeV } (1\sigma). \quad (14)$$

¹ If y^η is almost perturbative limit or the DM mass is localized at nearby the resonance of half of the SM Higgs mass, the relic density would be explained by itself.

Although η interacts with quark sector via Z -boson or Higgs boson at the tree level, it is easy to evade the constraints of direct detections. In case of interaction with Z -boson, which is inelastic scattering, the constraint would be evaded when the mass difference between η_R and η_I is more than 100 keV. In case of interaction with Higgs boson, which is elastic scattering, we can avoid the constraints if the Higgs coupling would be less than $\mathcal{O}(10^{-3})$.

This paper is organized as follows. In Sec. II, we review our model starting from the multiplication rules for our invertible symmetry, then constructing our valid Lagrangian, Higgs potential, radiative Dirac-type Yukawa terms, lepton flavor violations (LFVs), and muon $g-2$. In Sec. III, we discuss our DM candidates; N_{R_1} , S_0 , and η_R . Then, we demonstrate several numerical results for four cases of NH- S_0 DM, IH- S_0 DM, NH- η_R DM, IH- η_R DM in Sec. IV, satisfying neutrino observables, LFVs, muon $g-2$, relic density of DM. Finally, we summarize and conclude in Sec. V.

II. MODEL SETUP

Our model is to generate y_η at one-loop level. In order to achieve it, we introduce three isospin doublet vector-like fermions L' and singlet neutral boson S_0 , as well as N_R and η in the Ma model. In addition, we impose an invertible symmetry in the class under \mathbb{Z}_2 gauging of \mathbb{Z}_6 symmetry, which is denoted by $\mathcal{FR}(6)$, to each field. The fusion rules are as follows:

$$\begin{aligned} \epsilon \otimes \epsilon &= \mathbb{1} \oplus \sigma, & \sigma \otimes \sigma &= \mathbb{1} \oplus \sigma, & \rho \otimes \rho &= \mathbb{1}, \\ \epsilon \otimes \sigma &= \epsilon \oplus \rho, & \epsilon \otimes \rho &= \sigma, & \sigma \otimes \rho &= \epsilon. \end{aligned} \quad (15)$$

Therefore, following combinations of three fields

$$\epsilon \otimes \epsilon \otimes \sigma, \quad \sigma \otimes \sigma \otimes \sigma, \quad \epsilon \otimes \sigma \otimes \rho, \quad (16)$$

and those of four fields

$$\begin{aligned} \epsilon \otimes \epsilon \otimes \epsilon \otimes \epsilon, & \quad \epsilon \otimes \epsilon \otimes \epsilon \otimes \rho, & \quad \epsilon \otimes \epsilon \otimes \sigma \otimes \sigma, & \quad \epsilon \otimes \epsilon \otimes \rho \otimes \rho, \\ \epsilon \otimes \sigma \otimes \sigma \otimes \rho, & \quad \sigma \otimes \sigma \otimes \sigma \otimes \sigma, & \quad \sigma \otimes \sigma \otimes \rho \otimes \rho, & \quad \rho \otimes \rho \otimes \rho \otimes \rho, \end{aligned} \quad (17)$$

are invariant under the $\mathcal{FR}(6)$. Note here that all elements are commutable each other. The former controls the Yukawa and scalar trilinear couplings, and the latter for the scalar quartic couplings.

In Table II, we summarize all relevant particle contents as well as its charge assignments. Note that the quarks are all singlet under $\mathcal{FR}(6)$. According to this charge assignments, we add the following terms to Eq.(1):

$$f_{ib} \overline{L_{L_i}} L'_{R_b} S_0 + f'_{ab} \overline{L'_{L_a}} L'_{R_b} S_0 + g_{ab} \overline{L'_{L_a}} N_{R_b} \tilde{\eta} + h_{ab} \overline{L'_{R_a}} N_{R_b} \eta + M_{L'_b} \overline{L'_{L_b}} L'_{R_b} + \text{h.c.}, \quad (18)$$

Fields	Fermions					Scalars		
	L_L	ℓ_R	N_R	L'_L	L'_R	H	η	S_0
$SU(2)_L$	$\mathbb{2}$	$\mathbb{1}$	$\mathbb{1}$	$\mathbb{2}$	$\mathbb{2}$	$\mathbb{2}$	$\mathbb{2}$	$\mathbb{1}$
$U(1)_Y$	$-\frac{1}{2}$	-1	0	$-\frac{1}{2}$	$-\frac{1}{2}$	$\frac{1}{2}$	$\frac{1}{2}$	0
$\mathcal{FR}(6)$	$\mathbb{1}$	$\mathbb{1}$	ρ	σ	$\mathbb{1}$	ϵ	σ	

TABLE II: The charge assignments of relevant particles. Other particles not listed in this table have same SM charges with singlet under $\mathcal{FR}(6)$.

where $M_{L'}$ is diagonal without loss of generality. The scalar potential is found as follows:

$$\begin{aligned}
V = \sum_{\phi=H,\eta,S_0} & \left[-\mu_\phi^2 |\phi|^2 + \lambda_\phi |\phi|^4 \right] + \kappa_S S_0^3 + \left(\mu |\eta|^2 S_0 + \lambda''_{H\eta} (H^\dagger \eta)^2 + \text{c.c.} \right) \\
& + \lambda_{H\eta} |H|^2 |\eta|^2 + \lambda'_{H\eta} |H^\dagger \eta|^2 + \lambda_{HS} |H|^2 |S|^2 + \lambda_{\eta S} |\eta|^2 |S|^2.
\end{aligned} \tag{19}$$

Below, we move on to how to generate the Yukawa coupling y^η instead of discussing the scalar potential.

A. y^η at one-loop level

y^η is induced via terms f and g in Eq. (18) and μ in Eq. (19) at one-loop level, which is calculated as follows:

$$y_{ia}^\eta = \frac{\mu}{(4\pi)^2 (m_S^2 - m_0^2)} \sum_{b=1}^3 f_{ib} M_{L'_b} g_{ba} \left(\frac{m_S^2}{m_S^2 - M_{L'_b}^2} \ln \left[\frac{m_S^2}{M_{L'_a}^2} \right] - \frac{m_0^2}{m_0^2 - M_{L'_a}^2} \ln \left[\frac{m_0^2}{M_{L'_a}^2} \right] \right) \tag{20}$$

$$\equiv f_{ib} \widetilde{D}'_b g_{ba}. \tag{21}$$

where $m_0 \equiv (m_R + m_I)/2$. From Eq. (3) and Eq. (21), we can rewrite f and g as

$$f = U^* \sqrt{D_\nu} \left(\widetilde{D}' \right)^{-1/2}, \tag{22}$$

$$g = \left(\widetilde{D}' \right)^{-1/2} O_N D_N^{-1/2}, \tag{23}$$

where $\text{Max}[|f|] \lesssim 4\pi$ and $\text{Max}[|g|] \lesssim 4\pi$.

B. LVFs and muon $g - 2$

New contributions for LFVs arise from f and their formulae are simply given by changing $y^\eta \rightarrow f$, $m_\eta \rightarrow m_S$, $M_N \rightarrow M_{L'}$ in Eqs. (10) and (11) and flipping the overall sign². Therefore,

$$(a_R)_{ij} \approx -\frac{f_{ja}f_{ai}^\dagger m_{\ell_i}}{12(4\pi)^2} \left[\frac{M_{L'_a}^6 - 6M_{L'_a}^4 m_S^2 + 3M_{L'_a}^2 m_S^4 + 2m_S^2 + 6M_{L'_a}^2 m_S^4 \ln\left(\frac{M_{L'_a}^2}{m_S^2}\right)}{(M_{L'_a}^2 - m_S^2)^4} \right], \quad (24)$$

$$(a_L)_{ij} \approx -\frac{f_{ja}f_{ai}^\dagger m_{\ell_j}}{12(4\pi)^2} \left[\frac{M_{L'_a}^6 - 6M_{L'_a}^4 m_S^2 + 3M_{L'_a}^2 m_S^4 + 2m_S^2 + 6M_{L'_a}^2 m_S^4 \ln\left(\frac{M_{L'_a}^2}{m_S^2}\right)}{(M_{L'_a}^2 - m_S^2)^4} \right]. \quad (25)$$

From Eq. (9), this sign flipping leads to positive muon $g - 2$, which is clear difference from the Ma model.

III. DARK MATTER CANDIDATES

In our model, we have extra DM candidate from the Ma model, which is S_0 . Before showing our numerical results, we briefly summarize each feature in this section.

A. N_{R_1} DM

If we consider the fermion DM candidate, only the source to explain the relic density of DM is obtained via Yukawa couplings y^η , as mentioned in the introduction. However since y^η is generated at one-loop level, that would be tiny. In fact, we have found the maximum component of y^η is at most 10^{-4} for both the cases of NH and IH through our numerical analysis. On the other hand, the observed relic density of DM requires order one of y^η . Thus, the lightest mass of the neutral fermion cannot be a dominant component of the DM, and hence, we omit the numerical analysis for the fermion DM case in this paper.

² Sign flip comes from a fact that the photon attaches charged-fermions instead of charged-bosons.

B. S_0 DM

Here, we consider the isospin singlet DM candidate S_0 . For this purpose, we impose the following mass hierarchy

$$m_S < m_R, m_I, M_{N_1},$$

where m_R, m_I, M_{N_1} are masses of the other DM candidates and their analyses are done by several papers [34]. At first, we suppose the main annihilation cross section to explain the relic density of DM is arisen from Yukawa interaction via f . Moreover, the cross section can be expanded by relative velocity of v_{rel} : $\sigma v_{\text{rel}} \approx a_{\text{eff}} + b_{\text{eff}} v_{\text{rel}}^2 + d_{\text{eff}} v_{\text{rel}}^4 + \mathcal{O}(v_{\text{rel}}^6)$. Each coefficient is given by

$$a_{\text{eff}} = \sum_{b=1}^3 \frac{f_{3b} f_{b3}^\dagger}{8\pi} \frac{m_\tau^2}{(m_S^2 + M_{L'_b}^2 - m_\tau^2)^2} \theta(m_S - m_\tau), \quad (26)$$

$$b_{\text{eff}} = \sum_{b=1}^3 \frac{f_{3b} f_{b3}^\dagger}{24\pi} \frac{m_S^2 m_\tau^2 (m_\tau^2 - 3M_{L'_b}^2 - m_S^2)}{(m_S^2 + M_{L'_b}^2 - m_\tau^2)^4} \theta(m_S - m_\tau), \quad (27)$$

$$d_{\text{eff}} \approx \sum_{i,j=1}^3 \sum_{b=1}^3 \frac{f_{ib} f_{bj}^\dagger + \hat{f}_{ib} \hat{f}_{bj}^\dagger}{120\pi} \frac{m_S^6}{(m_S^2 + M_{L'_b}^2)^4}, \quad (28)$$

where $\hat{f} \equiv U^\dagger f$. The DM is d-wave dominant in the limit of zero mass of final states. The typical range of the cross section is given by

$$1.70630 \leq (\sigma v_{\text{rel}}) \times 10^9 \text{ GeV}^2 \leq 2.03102, \quad (29)$$

where it corresponds to $0.120 \pm 2 \times 0.001$ [29]. However, we have found that the DM would not reach the above cross section through our numerical analysis³. Thus, we need to rely on the other interactions arising from Higgs potential and kinetic terms. *One notice here is that S_0 can decay into a pair of the SM Higgses via μ and $\lambda_{H\eta}$ at one-loop level. Thus, we need to make them tiny enough to evade the too-short life time of S_0 when $250 \text{ GeV} \lesssim m_S$.*

C. η_R DM

In case of η_R DM, the main cross section would come from kinetic terms [36], since y^η is too small to explain the relic density as discussed in N_{R_1} DM candidate. Thus, the situation is the same as the case of original Ma model and we can adopt the same condition as can be seen in the

³ The annihilation is $\mathcal{O}(10^{-28}) \text{ GeV}^{-2}$ at most that is far below the required cross section.

introduction:

$$m_R \approx 534 \pm 8.5 \text{ GeV } (1\sigma). \quad (30)$$

η interacts with quark sector via Z -boson or Higgs boson at tree-level, and this case will suffer from the constraints of direct detections. As mentioned in the introduction, however, the constraints can be easily evaded by the enough mass difference between η_R and η_I (≥ 100 keV) for the Z -boson interaction case and small Higgs coupling ($\leq \mathcal{O}(10^{-3})$) for the Higgs boson interaction case. *Unlikely to the S_0 DM case, η never decay into the SM particles. This is because it is assured by \mathbb{Z}_2 symmetry originated from $\mathcal{FR}(6)$.*

IV. NUMERICAL RESULTS

In this section, we perform numerical analyses to satisfy the lepton masses and mixing angles, LFVs and muon $g-2$ where we adopt the best fit values of neutrino oscillation data in NuFit 6.0 [37] without Super-Kamiokande atmospheric data and charged-lepton masses in PDG [38]. Then, we check the allowed parameter space can also satisfy the relic density of DM for the cases of S_0 and η_R below. Before discussing the numerical analysis, it would be worthwhile mentioning the results of neutrino mass observables: $\sum D_\nu$, m_{ee} , $m_{\nu e}$, discussed in the introduction. When we impose $\sum D_\nu \leq 120$ meV and randomly select the lightest neutrino mass eigenvalue in the range of $D_{\nu 1}(D_{\nu 3}) \leq 1$ eV and two Majorana phases in the range of $(-\pi, \pi)$, we find the following upper bounds:

$$\text{NH} : \{D_{\nu 1}, m_{ee}, m_{\nu e}\} \lesssim \{30.031, 30.451, 31.305\} \text{ meV}, \quad (31)$$

$$\text{IH} : \{D_{\nu 3}, m_{ee}, m_{\nu e}\} \lesssim \{15.707, 50.910, 51.480\} \text{ meV}. \quad (32)$$

A. Numerical results of S_0 DM

We consider the DM candidate in case of S_0 and randomly select our input parameters in the following ranges:

$$\{m_S, \mu\} = [0.1 - 10^3] \text{ GeV}, \quad m_\eta = [m_S - 10^3] \text{ GeV}, \quad \{M_{N_1} \leq M_{N_2} \leq M_{N_3}\} = [m_S - 10^3] \text{ GeV}, \quad (33)$$

$$\{M_{L'_1} \leq M_{L'_2} \leq M_{L'_3}\} = [m_S - 10^3] \text{ GeV}, \quad |\theta_{12,23,13}| = [0.0 - \pi], \quad (34)$$

where $\theta_{12,23,13}$ are mixing angles of O_N .

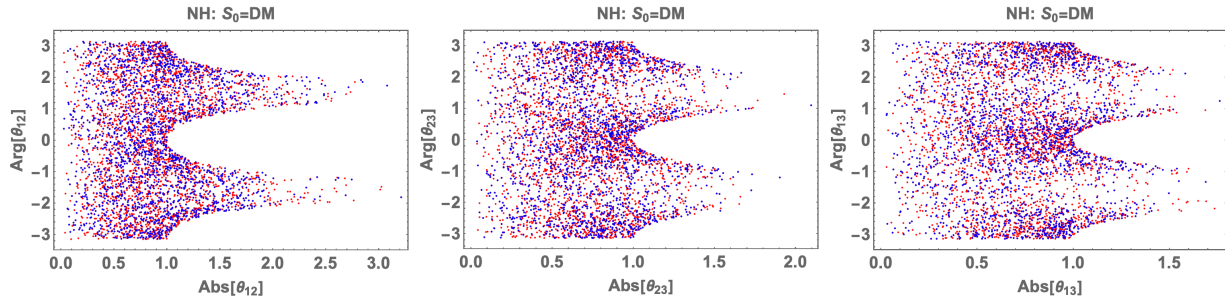


FIG. 1: Allowed regions for $\{\theta_{12}, \theta_{23}, \theta_{13}\}$, for the NH case with S_0 DM. Blue points are allowed only when $\sum D_\nu \leq 120$ meV is satisfied, otherwise points are colored by red. The vertical axis represents arguments, while the horizontal axis does the absolute values for these mixing angles.

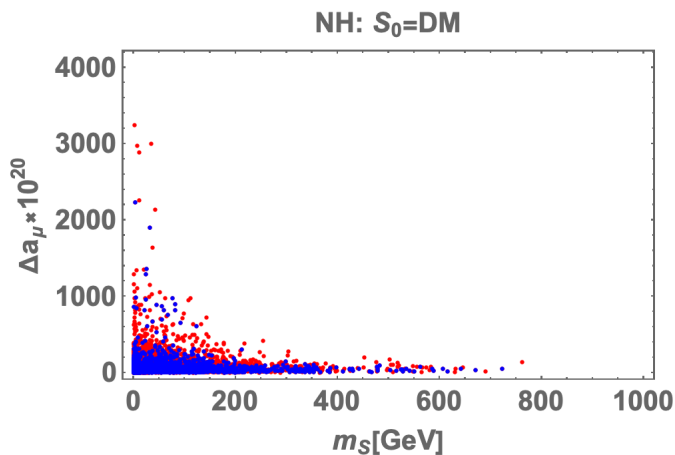


FIG. 2: Allowed regions for the muon $g - 2$ in terms of the DM mass, for the NH case with S_0 DM. All color legends are the same as the ones in Fig. 1.

1. NH

Fig. 1 shows allowed regions for θ_{12} (left), θ_{23} (center), θ_{13} (right) for the NH case. Blue points are allowed only when $\sum D_\nu \leq 120$ meV is satisfied, otherwise points are colored by red. Hereafter, we use this color legend for similar plots, without mentioning. The vertical axis represents arguments, while the horizontal axis does the absolute values for these mixing angles. These figures imply that they are unique shapes: all ranges for arguments are allowed for $\text{Abs}[\theta_{ij}] < 1.0$, while only specific regions are allowed for $\text{Abs}[\theta_{ij}] > 1.0$.

Fig. 2 shows allowed regions for muon $g - 2$ in terms of the mass of DM. As can be seen the figure, the predicted muon $g - 2$, $\Delta a_\mu \lesssim 3.2 \times 10^{-17}$, has almost no discrepancy from the SM prediction, and therefore, the result is consistent with the current discrepancy between theoretical

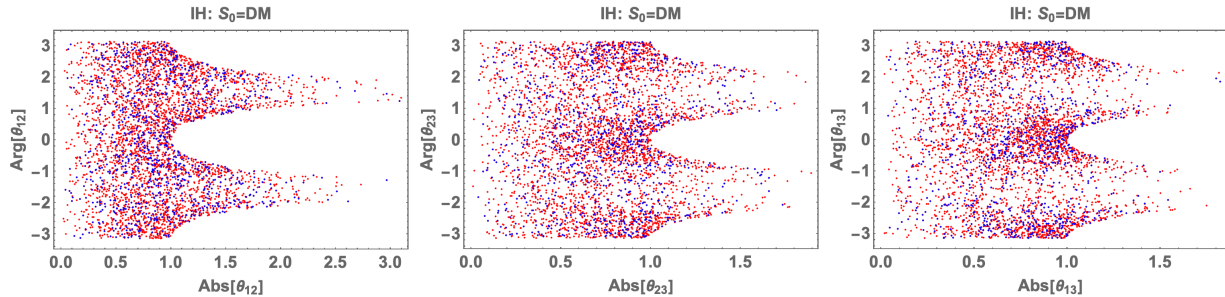


FIG. 3: Same plots as Fig. 1, for the IH case with S_0 DM.

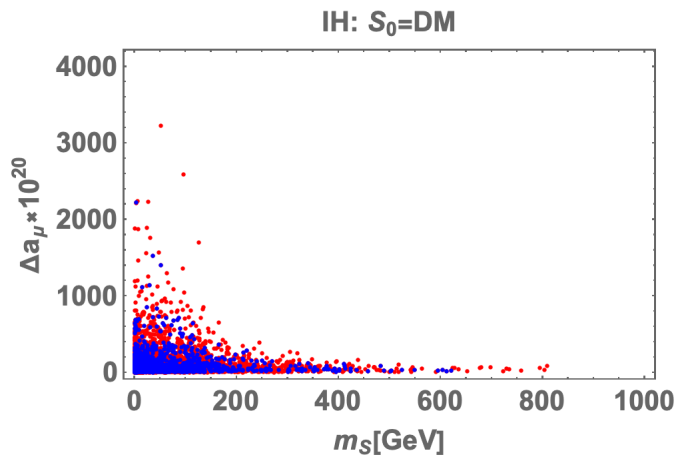


FIG. 4: Same plot as Fig. 2, for the IH case with S_0 DM.

and experimental results in Eq. (13). This figure shows another feature for our model: the upper bound on the DM mass is about 800 GeV.

2. IH

Fig. 3 shows allowed regions for θ_{12} (left), θ_{23} (center), θ_{13} (right) for the IH case. Comparing with Fig. 1, the shapes of allowed regions are similar with each other, while more points are out of $\sum D_\nu \leq 120$ meV.

Fig. 4 shows allowed regions for the muon $g - 2$ in terms of the mass of DM. Similar to the NH case, our muon $g - 2$ has almost no discrepancy from the SM prediction: $\Delta a_\mu \lesssim 3.2 \times 10^{-17}$, and the similar upper bound on the DM mass is obtained, $m_S \lesssim 800$ GeV.

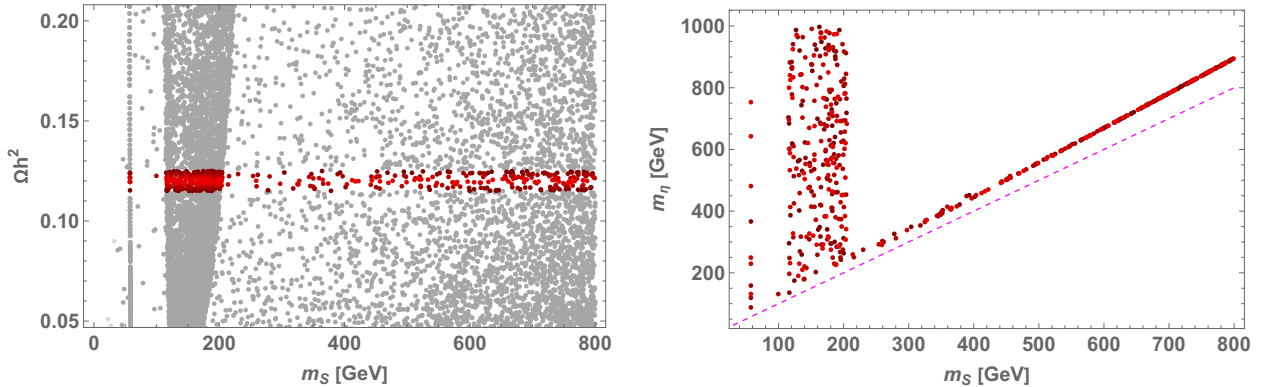


FIG. 5: Plots for the relic density in the case of the S_0 DM. *Left*: predicted relic density for each value of m_S ; *right*: relic density in the (m_S, m_η) -plane. We plot the DM relic density of $\Omega h^2 = 0.120 \pm 0.001$ [29] within $1\sigma, \dots, 5\sigma$ (in gradations of red from lighter to darker) and outside of 5σ (gray). In the right panel, we only plot the relic density within 5σ , and the magenta dashed line shows $m_S = m_\eta$. In both panels, the direct detection constraints are satisfied all points.

3. DM phenomenology

For the calculation of the relic density from S_0 DM, we simply neglect all Yukawa couplings in the calculation, and hence, the following results are common both for the NH and IH cases, as long as the contributions from these Yukawa couplings are enough small. We choose the relevant parameters as

$$m_\eta = [m_S - 10^3] \text{ GeV}, \quad m_S = [0 - 800] \text{ GeV}, \quad \{\kappa_S, \mu\} = [0 - 10^3] \text{ GeV}, \quad (35)$$

$$\lambda_{H\eta} = 0.1, \quad \lambda_{HS} = 0.001, \quad \lambda_{\eta S} = 0.0001, \quad (36)$$

and generate about 10^5 samples randomly. Here, the mass range for m_S is set be consistent with those obtained in previous results, and κ_S is a parameter for S_0^3 coupling, defined in Eq. (19). Note that other mass parameters m_{η^\pm}, m_I are set to be equal to $m_\eta = m_R$ for simplicity, which corresponds to the case of $\lambda'_{H\eta} = \lambda''_{H\eta} = 0$. Remaining quartic couplings λ_η, λ_S are totally irrelevant for the relic density calculation.

Fig. 5 shows our numerical results by using `micrOMEGAs` [39–43]⁴, in order for calculating the relic density as well as checking the direct detection bounds. In the left panel, the values of Ωh^2 for each DM mass are shown. The gray dots correspond to the case where predicted Ωh^2 is outside of 5σ of current result, $\Omega h^2 = 0.120 \pm 0.001$, while red plots indicate the prediction within $1\sigma, \dots, 5\sigma$

⁴ For more details, see <https://lapth.cnrs.fr/micromegas/>.

in gradation from lighter to darker. The right panel shows the predictions in (m_S, m_η) -plane, but only plot Ωh^2 within 5σ cases. Here, the effect from the loop decay of S_0 mentioned above is not included in the calculation, and therefore, some points in the range of $250 \text{ GeV} \leq m_S$ may disappear due to the short lifetime. Note that in these plots, all points satisfy the direct detection bounds.

From the right panel of Fig. 5, there are several critical DM mass ranges for this calculation: (i) $m_S \lesssim 100 \text{ GeV}$, (ii) $100 \text{ GeV} \lesssim m_S \lesssim 210 \text{ GeV}$ and (iii) $210 \text{ GeV} \lesssim m_S$.

(i) For this region, only $m_S \simeq 57.5 \text{ GeV}$ gives correct relic density, and the main annihilation mode is $S_0 S_0 \rightarrow b \bar{b}$ ($\simeq 86.5\%$), through the Higgs exchange. Sub-dominant ones are $S_0 S_0 \rightarrow \tau \bar{\tau}$ ($\simeq 9.1\%$) and $S_0 S_0 \rightarrow c \bar{c}$ ($\simeq 4.3\%$), which fixed by sizes of each SM Yukawa coupling.

(ii) For this region, the main annihilation becomes the ‘‘semi-annihilation’’ [44] of $S_0 S_0 \rightarrow S_0 h^0$ with the SM Higgs h^0 , depending on the size of m_η . When $m_\eta - m_S > 50 \text{ GeV}$, this semi-annihilation process is $\simeq 99.9\%$ of all relevant annihilation processes and determines the relic density of S_0 . On the other hand, once the mass relation becomes $m_\eta - m_S < 50 \text{ GeV}$, self-annihilation of $S_0 S_0 \rightarrow \eta^+ \eta^-$ and coannihilation of $S_0 \eta_{R,I} \rightarrow \eta^\pm W^\mp$ become relevant processes to the correct relic density. Note that for this region, how dominant process is obtained also depends on the size of κ_S and μ : enough size of $\kappa_S > \mu$ leads the self-annihilation to be dominant, while that of $\kappa_S < \mu$ leads the coannihilation dominant.

(iii) For this region, it is clear that the correct relic density is realized by the self-annihilation processes $S_0 S_0 \rightarrow \eta^+ \eta^-$, or the coannihilation ones $S_0 \eta_{R,I} \rightarrow \eta^\pm W^\mp$, depending on the size of κ_S and μ .

It is notable that these crucial DM mass ranges will be changed by choosing different choice for quartic couplings, $(\lambda_{H\eta}, \lambda_{HS}, \lambda_{\eta S})$. Among these, the size of λ_{HS} should be enough small, otherwise the direct detection bounds exclude almost all the viable parameter space.

B. Numerical results of η DM

Here, we consider the case of real part of η as the DM candidate. We work on the following DM mass range suggested by the ref. [36]:

$$m_R \approx 534 \pm 2 \times 8.5 \text{ GeV}, \quad (37)$$

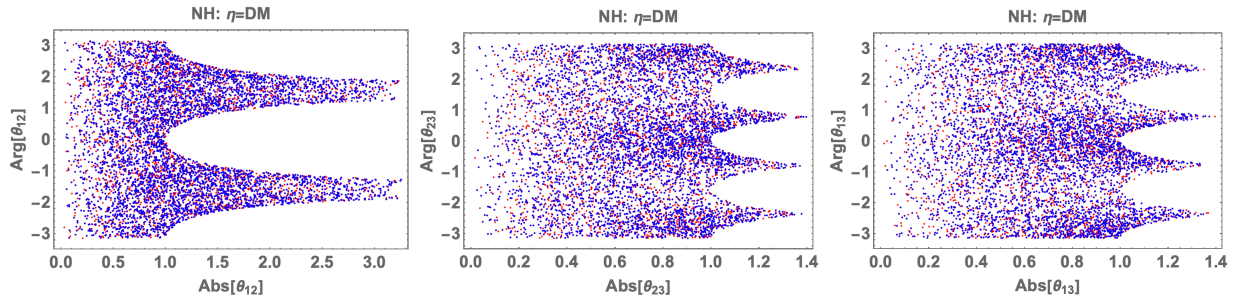


FIG. 6: Allowed regions for $\{\theta_{12}, \theta_{23}, \theta_{13}\}$, for the NH case with η DM.

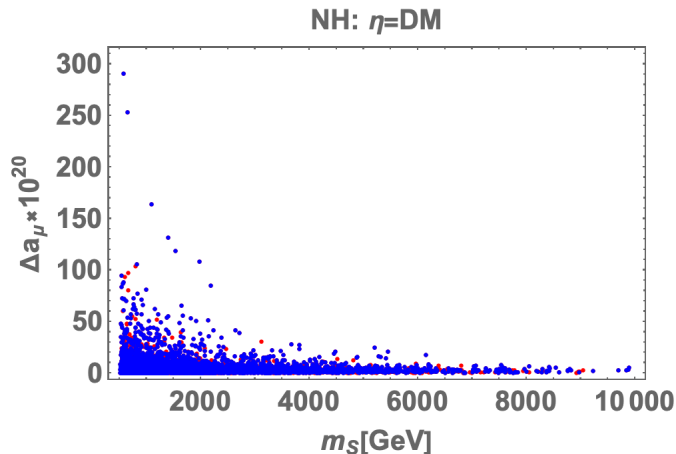


FIG. 7: Allowed regions for muon $g - 2$ in terms of the mass of DM where all the color legends are the same as the one of Fig. 1.

where m_R is the mass of η_R . Then, we randomly select our input parameters in the following ranges:

$$\{m_S, \mu\} = [0 - 10^4] \text{ GeV}, \quad \{M_{N_1} \leq M_{N_2} \leq M_{N_3}\} = [m_R - 10^4] \text{ GeV}, \quad (38)$$

$$\{M_{L'_1} \leq M_{L'_2} \leq M_{L'_3}\} = [m_R - 10^4] \text{ GeV}, \quad |\theta_{12,23,13}| = [0.0 - \pi]. \quad (39)$$

1. NH

Fig. 6 shows allowed regions for θ_{12} (left), θ_{23} (center), θ_{13} (right). The vertical axis represents arguments, while the horizontal axis does the absolute values for these mixing angles. These figures imply that allowed regions are similar to the S_0 DM case but there are two times of cusps for $\theta_{23,13}$ than the S_0 DM case. In addition, the maximum values of $\theta_{23,13}$ are smaller than those for the S_0 DM case. Furthermore, we obtained many more blue points, compared with the S_0 DM case, both

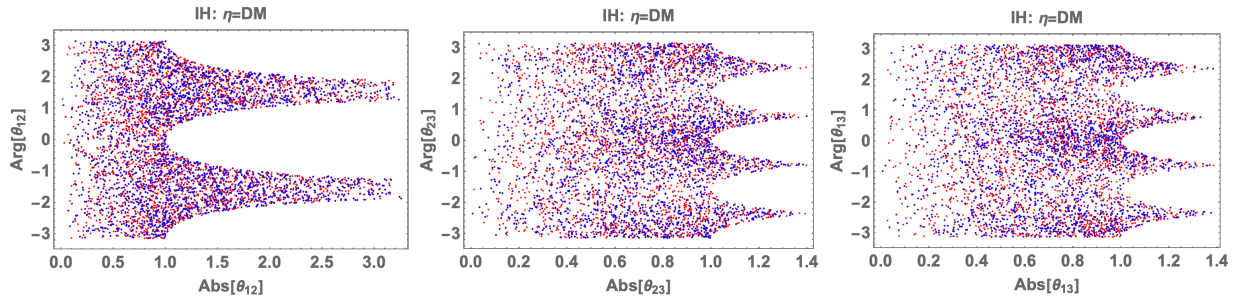


FIG. 8: Same plot as Fig. 6, for the IH case with η DM.

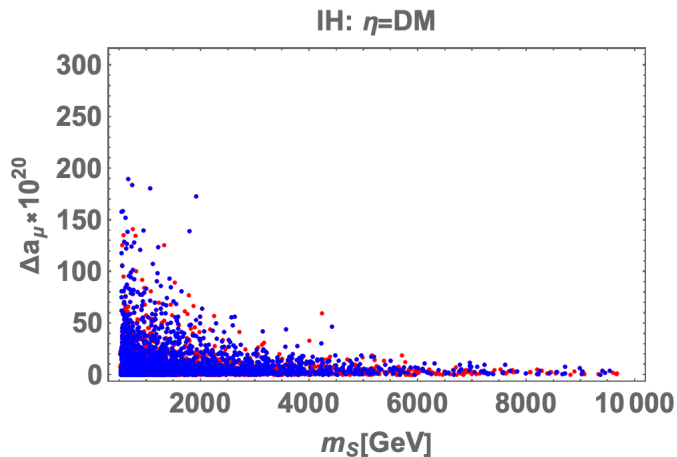


FIG. 9: Same plot as Fig. 7, for the IH case with η DM.

of the NH and IH cases. This will be originated from the heavy mass of m_S , which is $m_S \gtrsim 534$ GeV for the current case.

Fig. 7 shows allowed regions for muon $g - 2$ in terms of the mass of DM. As can be seen the figure, the muon $g - 2$, $\Delta a_\mu \lesssim 3.0 \times 10^{-18}$, has almost no discrepancy from the SM prediction, and the predictions tend to be smaller than that of the S_0 DM case, due to the large mass of S_0 . Different from the S_0 DM case, m_S mass runs whole the range within our fixed range.

2. IH

Fig. 8 shows allowed regions for θ_{12} (left), θ_{23} (center), θ_{13} (right). Similar to the NH case, these figures imply that these shapes are almost the same as the NH one but more points are out of $\sum D_\nu \leq 120$ meV, as we observed in the S_0 DM case. However, the number of blue points is larger than that of the IH case with S_0 DM.

Fig. 9 shows allowed regions for the muon $g - 2$ in terms of the mass of DM. Similar to the NH case, the muon $g - 2$ has almost no discrepancy from the SM prediction; $\Delta a_\mu \lesssim 2.0 \times 10^{-18}$. Again, m_S mass runs whole the range within our fixed range, and the similar conclusion in the NH case for the muon $g - 2$ prediction can be seen in the figure.

V. SUMMARY AND DISCUSSION

We have proposed a radiatively induced neutrino masses at the three-loop level, based on the Ma model. We introduced a non-invertible symmetry in the class under the \mathbb{Z}_2 gauging of \mathbb{Z}_6 symmetry and added three isospin doublet vector-like fermions L' and singlet boson S_0 . The Yukawa interactions directly related to the neutrino masses are forbidden at the tree-level, under this symmetry. However, the terms are allowed at one-loop level due to L' and S_0 as well as η , which is no longer invariant under this symmetry any more. Therefore, the symmetry is dynamically broken. Interestingly, η contributes to both the radiative matrices y^η and m_ν .

Under the model set, we have performed numerical analyses to satisfy the lepton flavor violations, muon $g - 2$, and boson DM candidates S_0 and η_R for the cases of NH and IH. Then, we have shown allowed parameter space for our model in four cases and concluded all the cases have almost same results except the DM candidate. Although there are similarity in the results, we have found specific features for each DM case, especially in the results of $\text{Abs}[\theta_{23,13}] > 1.0$.

Acknowledgments

HO is supported by Zhongyuan Talent (Talent Recruitment Series) Foreign Experts Project. YS is supported by Natural Science Foundation of China under grant No. W2433006.

-
- [1] Y. Choi, H. T. Lam, and S.-H. Shao, Phys. Rev. Lett. **129**, 161601 (2022), 2205.05086.
 - [2] C. Cordova, S. Hong, S. Koren, and K. Ohmori, Phys. Rev. X **14**, 031033 (2024), 2211.07639.
 - [3] C. Cordova and K. Ohmori, Phys. Rev. X **13**, 011034 (2023), 2205.06243.
 - [4] C. Cordova, S. Hong, and S. Koren (2024), 2402.12453.
 - [5] T. Kobayashi, H. Otsuka, and M. Tanimoto, JHEP **12**, 117 (2024), 2409.05270.
 - [6] T. Kobayashi and H. Otsuka, JHEP **11**, 120 (2024), 2408.13984.
 - [7] T. Kobayashi, Y. Nishioka, H. Otsuka, and M. Tanimoto, JHEP **05**, 177 (2025), 2503.09966.
 - [8] M. Suzuki and L.-X. Xu (2025), 2503.19964.

- [9] Q. Liang and T. T. Yanagida (2025), 2505.05142.
- [10] T. Kobayashi, H. Otsuka, M. Tanimoto, and H. Uchida (2025), 2505.07262.
- [11] T. Kobayashi, H. Mita, H. Otsuka, and R. Sakuma (2025), 2506.10241.
- [12] T. Kobayashi, H. Okada, and H. Otsuka (2025), 2505.14878.
- [13] T. Nomura and H. Okada (2025), 2506.16706.
- [14] J. Dong, T. Jeric, T. Kobayashi, R. Nishida, and H. Otsuka (2025), 2507.02375.
- [15] T. Nomura and O. Popov (2025), 2507.10299.
- [16] J. Chen, C.-Q. Geng, H. Okada, and J.-J. Wu (2025), 2507.11951.
- [17] L. Bhardwaj and Y. Tachikawa, *JHEP* **03**, 189 (2018), 1704.02330.
- [18] R. Dijkgraaf, E. P. Verlinde, and H. L. Verlinde, *Commun. Math. Phys.* **115**, 649 (1988).
- [19] T. Kobayashi, S. Raby, and R.-J. Zhang, *Nucl. Phys. B* **704**, 3 (2005), hep-ph/0409098.
- [20] T. Kobayashi, H. P. Nilles, F. Ploger, S. Raby, and M. Ratz, *Nucl. Phys. B* **768**, 135 (2007), hep-ph/0611020.
- [21] F. Beye, T. Kobayashi, and S. Kuwakino, *Phys. Lett. B* **736**, 433 (2014), 1406.4660.
- [22] R. Thorngren and Y. Wang, *JHEP* **07**, 051 (2024), 2106.12577.
- [23] J. J. Heckman, J. McNamara, M. Montero, A. Sharon, C. Vafa, and I. Valenzuela (2024), 2402.00118.
- [24] J. Kaidi, Y. Tachikawa, and H. Y. Zhang (2024), 2402.00105.
- [25] J. Dong, T. Kobayashi, R. Nishida, S. Nishimura, and H. Otsuka (2025), 2504.09773.
- [26] S. Funakoshi, T. Kobayashi, and H. Otsuka (2024), 2412.12524.
- [27] E. Ma, *Phys. Rev. D* **73**, 077301 (2006), hep-ph/0601225.
- [28] J. A. Casas and A. Ibarra, *Nucl. Phys. B* **618**, 171 (2001), hep-ph/0103065.
- [29] N. Aghanim et al. (Planck), *Astron. Astrophys.* **641**, A6 (2020), [Erratum: *Astron. Astrophys.* 652, C4 (2021)], 1807.06209.
- [30] S. Abe et al. (KamLAND-Zen) (2024), 2406.11438.
- [31] M. Aker et al. (KATRIN), *Science* **388**, adq9592 (2025), 2406.13516.
- [32] D. P. Aguillard et al. (Muon g-2) (2025), 2506.03069.
- [33] R. Aliberti et al. (2025), 2505.21476.
- [34] J. Kubo, E. Ma, and D. Suematsu, *Phys. Lett. B* **642**, 18 (2006), hep-ph/0604114.
- [35] P. A. R. Ade et al. (Planck), *Astron. Astrophys.* **594**, A13 (2016), 1502.01589.
- [36] T. Hambye, F. S. Ling, L. Lopez Honorez, and J. Rocher, *JHEP* **07**, 090 (2009), [Erratum: *JHEP* 05, 066 (2010)], 0903.4010.
- [37] I. Esteban, M. C. Gonzalez-Garcia, M. Maltoni, I. Martinez-Soler, J. a. P. Pinheiro, and T. Schwetz, *JHEP* **12**, 216 (2024), 2410.05380.
- [38] R. L. Workman et al. (Particle Data Group), *PTEP* **2022**, 083C01 (2022).
- [39] G. Bélanger, F. Boudjema, A. Goudelis, A. Pukhov, and B. Zaldivar, *Comput. Phys. Commun.* **231**, 173 (2018), 1801.03509.
- [40] G. Belanger, A. Mjallal, and A. Pukhov, *Eur. Phys. J. C* **81**, 239 (2021), 2003.08621.

- [41] G. Belanger et al., JHEP **02**, 042 (2022), 2111.08027.
- [42] G. Alguero, G. Belanger, S. Kraml, and A. Pukhov, SciPost Phys. **13**, 124 (2022), 2207.10536.
- [43] G. Alguero, G. Belanger, F. Boudjema, S. Chakraborti, A. Goudelis, S. Kraml, A. Mjallal, and A. Pukhov, Comput. Phys. Commun. **299**, 109133 (2024), 2312.14894.
- [44] F. D'Eramo and J. Thaler, JHEP **06**, 109 (2010), 1003.5912.